Road Centerline Extraction via Semisupervised Segmentation and Multidirection Nonmaximum Suppression

Guangliang Cheng, Feiyun Zhu, Shiming Xiang, and Chunhong Pan

***Abstract*—Accurate road centerline extraction from remotely sensed images plays a significant role in road map generation and updating. In the road extraction problem, the acquisition of labeled data is time consuming and costly; thus, there are only a small amount of labeled samples in reality. In the existing centerline extraction algorithms, the thinning-based algorithms always produce small spurs that reduce the smoothness and accuracy of the road centerline; the regression-based algorithms can extract a smooth road network, but they are time consuming. To solve the aforementioned problems, we propose a novel road centerline extraction method, which is constructed based on semisupervised segmentation and multiscale filtering (MF) and multidirection nonmaximum suppression (M-NMS) (MF&M-NMS). Specifically, a semisupervised method, which explores the intrinsic structures between the labeled samples and the unlabeled ones, is introduced to obtain the segmentation result. Then, a novel MF&M-NMS-based algorithm is proposed to gain a smooth and complete road centerline network. Experimental results on a public data set demonstrate that the proposed method achieves comparable or better performances by comparing with the state-of-the-art methods. In addition, our method is nearly ten times faster than the state-of-the-art methods.**

***Index Terms*—Multidirection nonmaximum suppression (M-NMS), multiscale filtering (MF), road centerline extraction, semisupervised segmentation.**

I. Introduction

ROAD centerline extraction from remotely sensed imagery has been an active research due to its vital applications in urban planning, vehicle navigation, intelligent transportation system, etc. Although various approaches [1]–[3] have been proposed to address this task, it is still challenging to obtain both smooth and complete road network.

For most existing road centerline extraction methods [4]–[6], two steps are included to obtain the final road network. First, different kinds of algorithms are employed to obtain the homogeneous road area result. Then, a centerline extraction algorithm is used to get the final road centerline network.

Manuscript received September 10, 2015; revised December 13, 2015 and January 26, 2016; accepted January 27, 2016. Date of publication February 19, 2016; date of current version March 23, 2016. This work was supported by the Natural Science Foundation of China under Grants 91338202, 91438105, 61305049, and 61370039.

The authors are with the National Laboratory of Pattern Recognition, Institute of Automation, Chinese Academy of Sciences, Beijing 100190, China (e-mail: guangliang.cheng@nlpr.ia.ac.cn; fyzhu@nlpr.ia.ac.cn; smxiang@nlpr.ia.ac.cn; chpan@nlpr.ia.ac.cn).

Color versions of one or more of the figures in this paper are available online at http://ieeexplore.ieee.org.

Digital Object Identifier 10.1109/LGRS.2016.2524025

In the road area extraction problem, supervised classification algorithms [4], [7], [8] were widely used. A support vector machine (SVM)-based road network extraction method was proposed by Shi *et al.* [4], in which spectral–spatial classification and shape features were employed. Cheng *et al.* [7] presented a graph cut-based road extraction approach, in which SVM-based probability propagation and spatial information were integrated. Mnih and Hinton [8] proposed a deep neural network-based method to extract the urban road network from high-resolution images. Although these supervised classification-based methods have achieved great results, a large amount of labeled samples are needed to train these classifiers. However, manually labeled samples are expensive and difficult to acquire. In most cases, we only have a small set of labeled samples and a large collection of unlabeled ones.

For the road centerline extraction problem, the morphological thinning algorithm [5], [6] was widely used because it is fast and easy to implement. However, the thinning-based algorithm always produces short spurs and brings in many false positives, which reduce the smoothness and accuracy of the road network. To alleviate these problems, some regression-based centerline extraction algorithms [4], [9] have been introduced. Although these algorithms can extract smooth and accurate road centerlines, they also have two shortcomings: 1) they are ineffective to extract the centerlines around the road intersections, and 2) they are time consuming.

To solve the problem of limited labeled samples, inspired by Nie *et al.* [10], we propose a semisupervised road area extraction algorithm, which incorporates the information of both labeled and unlabeled samples. Then, to overcome the aforementioned shortcomings of centerline extraction algorithms, a multiscale filtering (MF) and multidirection nonmaximum suppression (M-NMS) (MF&M-NMS) algorithm is proposed. The main contributions of our approach are highlighted as follows.

1) A new semisupervised road area extraction algorithm is proposed. By exploring the intrinsic structures between the labeled samples and unlabeled ones, it greatly improves the road extraction performance with limited labeled samples.
2) A novel MF&M-NMS-based road centerline extraction algorithm is proposed. On the one hand, this algorithm can extract a smooth road network with little processing time. On the other hand, it can overcome the shortcoming of existing regression-based algorithms in the road intersections; thus, it can obtain a complete road network.

The remainder of this letter is arranged as follows. Section II presents the proposed methodology. Experimental evaluations

and detailed comparisons are reported in Section III. Conclusions are drawn in Section IV.

II. Proposed Methodology

The proposed road extraction approach consists of three steps: object-based feature extraction, semisupervised segmentation, and MF&M-NMS-based road centerline extraction.

A. Object-Based Feature Extraction

In this letter, to reduce the side influence of occlusions and to extract the geometric characteristics of road regions, the object-oriented algorithm is employed to extract the contextual features of road regions. Although other choices are also feasible, here, we use the mean shift [11] algorithm to generate superpixels, which are treated as objects. Mean shift runs fast and can preserve the road boundaries well.

In this letter, inspired by Cheng *et al.* [12], we utilize three types of features: spectral features, geometric and texture features, and contextual features. They are defined as follows.

Spectral Features: As the pixels within one superpixel tend to have similar spectral characteristics, thus, we define the spectral attribute of a superpixel as the average spectral value within this superpixel.

Geometric and Texture Features: The extended multiattribute profile (EMAP) [13] was widely used to capture the geometric and texture features in hyperspectral image analysis. EMAP captures the spatial information via morphological attribute filters, such as area, diagonal of the bounding box of the region, etc. Here, we extract the EMAP features for all the pixels in the image, and then, we calculate the EMAP feature of a superpixel as the mean value of the EMAP features in this superpixel.

It should be noted that we normalize the aforementioned two features, respectively. Then, we concatenate them as the feature of the superpixel. To enhance the discriminative power of each superpixel, the spatially adjacent superpixels should be considered, which is defined as contextual information as follows.

Contextual Features: Intuitively, road regions are connected together. In most cases, for a road superpixel, there are at least two road superpixels in its spatially neighboring superpixels. Among all the spatially neighboring superpixels of the center superpixel, we find out the two superpixels which are the first two closest superpixels to the center superpixel in the concatenated feature space. Then, we concatenate them as the contextual feature for the center superpixel.

B. Semisupervised Segmentation

Suppose that we have obtained N superpixels after oversegmentation. For clarity, we denote the ith superpixel by $\mathbf{x}_i \in \mathbb{R}^m$ $(i = 1, 2, \ldots, N)$, where m is the dimension of the features. In semisupervised learning, only limited labeled samples are available. Without loss of generality, suppose that the first l samples $\mathbf{x}_1, \mathbf{x}_2, \ldots, \mathbf{x}_l$ are labeled and the others are unlabeled. Denote $\mathbf{X} = [\mathbf{x}_1, \mathbf{x}_2, \ldots, \mathbf{x}_N] \in \mathbb{R}^{m\times N}$ as the feature matrix for all the samples. For the two-class classification problem, we denote the label of the positive samples (road class) by 1 and that of the negative samples (nonroad class) by -1. Let $\mathbf{f}_{(l)} = [y_1, y_2, \ldots, y_l]^T$ denote the label vector of the labeled samples. For those unlabeled samples, we denote its initial label as 0. Let $\mathbf{f}_{(u)}$ denote the predicted label vector for those unlabeled samples. Denote the predicted label vector by $\mathbf{f} = \begin{bmatrix}\mathbf{f}_{(l)}\\ \mathbf{f}_{(u)}\end{bmatrix} \in \mathbb{R}^N$.

Problem Formalization: In our method, the road segmentation problem is studied in a semisupervised framework via a regression-based algorithm. The model can be described as follows:

$$\arg\min_{\mathbf{w},\mathbf{f},b} \sum_{i=1}^{l} \|\mathbf{w}^T\mathbf{x}_i + b - y_i\|_2^2 + \lambda \sum_{i=l+1}^{N} \|\mathbf{w}^T\mathbf{x}_i + b - y_i\|_2^2 + \alpha(\mathbf{f}^T\mathbf{L}\mathbf{f}) + \beta\|\mathbf{w}\|_2^2 \quad (1)$$

where $\mathbf{w} \in \mathbb{R}^m$ and b are the projection vector and bias scatter, respectively; λ, α, and β are hyperparameters, where λ controls the relative significance of the labeled samples and the unlabeled samples. $\mathbf{L} \in \mathbb{R}^{N\times N}$ is a Laplacian matrix on the graph, which is calculated by $\mathbf{L} = \mathbf{D} - \mathbf{S}$. $\mathbf{S}$ is a similarity matrix, which is calculated to encode the similarity between sample pairs via *k-nearest neighbor* and heat kernel function [14]. $\mathbf{D}$ is a diagonal matrix, whose ith diagonal element is calculated by $d_{ii} = \sum_j s_{ij}$. The first term and the second term in (1) are regression errors for the labeled samples and unlabeled ones, respectively. The third term is a graph-based manifold regularization, which is to enhance the label smoothness between the samples. The regularization term $\|\mathbf{w}\|_2^2$ is used to avoid overfitting.

In (1), the first two terms can be combined; thus, a concise formulation can be defined as

$$\mathcal{L} = \left(\mathbf{X}_a^T\mathbf{w}_a - \mathbf{f}\right)^T \mathbf{\Lambda} \left(\mathbf{X}_a^T\mathbf{w}_a - \mathbf{f}\right) + \alpha(\mathbf{f}^T\mathbf{L}\mathbf{f}) + \beta\mathbf{w}_a^T\mathbf{w}_a \quad (2)$$

where $\mathbf{X}_a = [\mathbf{X}; \mathbf{1}^T] \in \mathbb{R}^{(m+1)\times N}$ is an augmented matrix, in which $\mathbf{1}$ is a vector with all the elements as one. Accordingly, $\mathbf{w}_a = [\mathbf{w}; b] \in \mathbb{R}^{m+1}$ is an augmented vector; $\mathbf{\Lambda} = \mathrm{diag}\{1, 1, \ldots, \lambda, \lambda\} \in \mathbb{R}^{N\times N}$ is a diagonal weight matrix for all the samples.

The objective function in (2) is convex and differentiable with respect to $\mathbf{f}$ and $\mathbf{w}_a$. Thus, the optimum is expected to be achieved. In this letter, an iterative update algorithm is employed to find the optimal solution.

Optimization: Fixing $\mathbf{f}$, taking the derivative of $\mathcal{L}$ with respect to $\mathbf{w}_a$, we obtain

$$\frac{\partial\mathcal{L}}{\partial\mathbf{w}_a} = 2\mathbf{X}_a\mathbf{\Lambda}\mathbf{X}_a^T\mathbf{w}_a - 2\mathbf{X}_a\mathbf{\Lambda}\mathbf{f} + 2\beta\mathbf{w}_a. \quad (3)$$

Let $\partial\mathcal{L}/\partial\mathbf{w}_a = 0$, and we get

$$\mathbf{w}_a = \left(\mathbf{X}_a\mathbf{\Lambda}\mathbf{X}_a^T + \beta\mathbf{I}_{(m+1)}\right)^{-1}\mathbf{X}_a\mathbf{\Lambda}\mathbf{f} \quad (4)$$

where $\mathbf{I}_{(m+1)}$ is an $(m+1)\times(m+1)$ identity matrix.

Fixing $\mathbf{w}_a$, taking the derivative of $\mathcal{L}$ with respect to $\mathbf{f}$, we obtain

$$\frac{\partial\mathcal{L}}{\partial\mathbf{f}} = -2\mathbf{\Lambda}\mathbf{X}_a^T\mathbf{w}_a + 2\mathbf{\Lambda}\mathbf{f} + 2\alpha\mathbf{L}\mathbf{f}. \quad (5)$$

Let $\partial\mathcal{L}/\partial\mathbf{f} = 0$, and we obtain

$$\mathbf{f} = (\mathbf{\Lambda} + \alpha\mathbf{L})^{-1}\mathbf{\Lambda}\mathbf{X}_a^T\mathbf{w}_a. \quad (6)$$

Algorithm 1: Semisupervised road segmentation.

Input:
The object-based feature matrix of the image $\mathbf{X}_a$;
The label vector for the labeled instances $\mathbf{f}_{(l)}$;
Parameter λ, α and β.
Output:
Pixel-based road segmentation result.
1: Initialize $\mathbf{f}$ and $\mathbf{w}_a$.
2: Calculate the graph-based Laplacian matrix $\mathbf{L}$.
3: **repeat**
4: Update $\mathbf{w}_a$ by the updating rule (4).
5: Update $\mathbf{f}$ by the updating rule (6).
6: **until** Convergence
7: Obtain the object-based label via Eq. (7).
8: Obtain the pixel-based label according to the rule (II-B).
9: **return** Pixel-based road segmentation result.

By iteratively updating $\mathbf{w}_a$ and $\mathbf{f}$, when the changes of the two values lie within a very small scope, the optimization process converges.

After the iterative update, we get the predicted label matrix. Then, we classify an unlabeled sample $\mathbf{x}_i$ $(l+1 < i < N)$ with a threshold τ (usually, we set $\tau = 0$) according to the following rule:

$$l(\mathbf{x}_i) = \begin{cases} 1 & \text{if } f(\mathbf{x}_i) \geq \tau \\ -1 & \text{else.} \end{cases} \tag{7}$$

After obtaining the final labels for all the superpixels, all the pixel labels are obtained according to the rule II-B: All the pixels in the same superpixel are given the same label value as the superpixel. The semisupervised road segmentation algorithm is summarized in Algorithm 1.

After the segmentation, many roadlike segments (i.e., roofs, parking lots, etc.) are also included in the final segmentation result. To distinguish between potential road segments and roadlike segments, the elimination algorithm with road-geometrical prior [7] is employed. After this process, only the road segments remain.

C. Road Centerline Extraction via MF&M-NMS

In the road centerline extraction problem, the traditional morphological thinning algorithm was widely used because it is fast and easy to implement. However, it always produces short spurs and brings in many false positives. To overcome this shortcoming, regression-based algorithms [4], [9] were performed to obtain smooth road centerlines, but they are time consuming. To solve the aforementioned problems, an MF&M-NMS-based road centerline extraction algorithm is proposed. It has two strengths: 1) It does not produce spurs, and 2) it is fast and easy to be realized.

MF: For the segmentation result, we continuously filter the image with different kernel sizes. Specifically, at the first, we filter the image with a larger filter size, and then, we use the filters in the declining size. This is behind the motivation that, after the aforementioned continuous filtering, the real road centerline positions tend to have local maximum values. Thus, the MF can be defined as

$$\mathbf{I}^{(s+1)} = \mathbf{I}^{(s)} * \mathbf{F}^{(s+1)} \tag{8}$$

where s denotes the sth filtering, $\mathbf{I}^{(0)}$ denotes the segmentation result without any filtering, $*$ denotes the convolution operation, and $\mathbf{F}$ denotes the convolution kernel. Here, we use the Gaussian kernel. Intuitively, the maximal kernel size should be larger than the road width, and then, we decrease the kernel size to 3 at the step of 2. After that, local maximum values accumulate to road centerline positions. As Fig. 1(b) shows, the centerline positions are lighter than the surrounding areas. Thus, it demonstrates that the MF algorithm is effective to accumulate the maximum values to road centerline positions.

M-NMS: To get the complete and smooth road centerline network, nonmaximum suppression (NMS) algorithm is applied. The NMS only retains those locations which are the local maximum along a line perpendicular to the local orientation within a neighborhood of width. We found that the road network is incomplete when only using one certain orientation. Thus, in our experiments, we use the NMS in eight different orientations (0, 45°, 90°, 135°, 180°, 225°, 270°, and 315°). As Fig. 1(c) shows, we obtain road centerline results from eight different NMS orientations. As we can see, although some centerline parts are detected more than once, these eight centerline extraction results complement each other.

Combination: After we have obtained eight road centerline extraction results, a combination rule should be proposed to integrate these results. Here, we combine the results according to the following rules.

1) We eliminate the centerlines with less than T pixels. Because roads are continuous and connected with each other, thus short centerlines tend to be nonroad part.
2) Only those locations which are detected more than twice are retained on the final road centerline network.

After the aforementioned process, we get the final road centerline network. As Fig. 1(d) shows, the centerline network is smooth and complete by employing the MF&M-NMS algorithm.

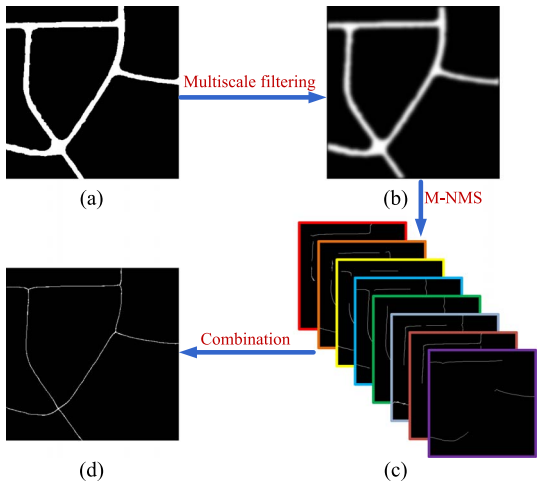

Fig. 1. Flowchart of the proposed road centerline extraction method. (a) Road segmentation result. (b) Result after MF. (c) Result after M-NMS. (d) Final centerline result.

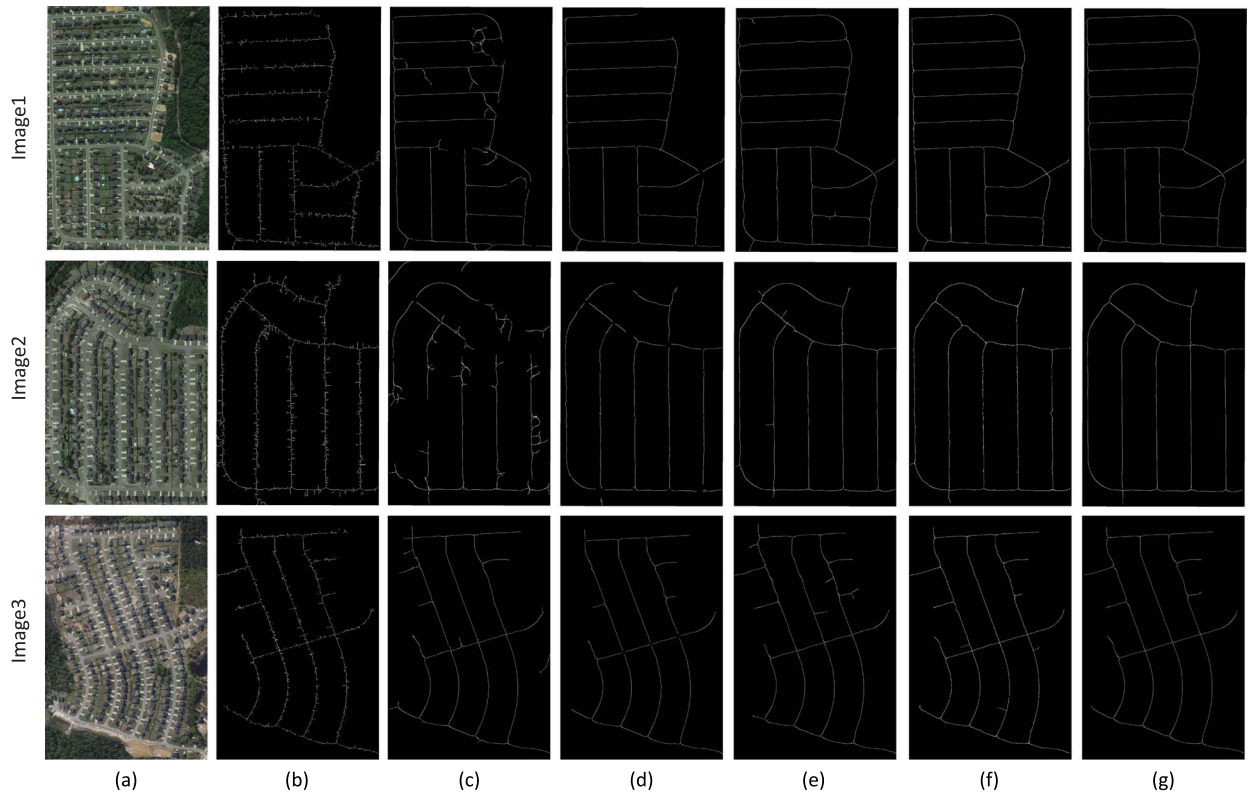

Fig. 2. Visual comparisons of road centerline extraction results. From left to right: (a) Original image, (b) result of Huang [5], (c) result of Miao [9], (d) result of Shi [4], (e) result of Cheng [12], (f) result of proposed method, and (g) reference map. Due to the space limit, we only display three images.

III. Experimental Results

To verify the effectiveness of our method, visual and quantitative performances are compared with that of other state-of-the-art methods. Due to the space limit, we only display three images.

A. Data Sets

We use the road centerline extraction data set provided by Cheng *et al.* [12] to test the proposed method. In this data set, there are 30 images with the spatial resolution of 1.2 m per pixel. Most of the images are under complex backgrounds and occlusions of cars and trees.

B. Compared Methods

To test the performances of the proposed method, we compared our approach with state-of-the-art road centerline extraction methods. They are Huang's method (Huang) [5], Miao's method (Miao) [9], Shi's method (Shi) [4], and Cheng's method (Cheng) [12].

C. Quality Evaluation

To evaluate the performance of the road centerline extraction methods, *completeness* (com), *correctness* (cor), and *quality* (q) [15] are used in this letter. Due to the deviation between the manually labeled centerline and the real centerline, "buffer width" [16] is introduced to calculate these metrics. In the experiments, we set the buffer width as 2 pixels.

D. Parameter Setting

For the mean shift, we set $(h_s, h_r, M) = (7, 5, 100)$, where h_s and h_r are bandwidth parameters in the spatial and range domains and M is the minimum size of each superpixel. In our experiments, we set $\beta = 1$. Intuitively, the relative importance of the unlabeled samples should be smaller than that of the labeled samples; thus, we set $\lambda = 0.6$. We tune the parameter α via cross-validations. In the MF step, we employ the filtering window size from 19 to 3 at the interval of 2 pixels. In the M-NMS step, we set the window size of NMS as 20 and $T = 10$ for all the experiments.

E. Performance Evaluation

Visual Comparisons: Fig. 2 shows the comparing results of different methods in visual performance. Cheng's method and the proposed method gain better performance than the other three methods. Huang's method produces more small spurs than the other methods. Miao's method produces some false positives because it is hard for this method to distinguish the homogeneous areas from real road areas. In addition, Miao's method and Shi's method are not effective to extract the centerlines in the road intersections.

Quantitative Comparisons: Table I shows the quantitative performance of the sample images and average performance of all the 30 images in the data set. As we can see, the proposed method is comparable to or better than Cheng's method, which gains the best performance among the comparing methods. Huang's method and Miao's method obtain relatively poor results because there are a lot of false positives.

TABLE I
QUANTITATIVE COMPARISONS AMONG DIFFERENT METHODS, WHERE THE VALUES IN BOLD TEXT ARE THE BEST AND THE VALUES IN BOLD ITALIC TEXT ARE THE SECOND BEST. IT SHOULD BE NOTED THAT THE LAST COLUMN IS THE AVERAGE PERFORMANCE OF ALL IMAGES IN THE DATA SET

		Huang	Miao	Shi	Cheng	Proposed
Image1	com	*0.9763*	0.9064	0.9204	0.9651	**0.9885**
	cor	0.6362	0.7801	**0.9791**	*0.9370*	0.9212
	q	0.6265	0.7219	0.9027	*0.9063*	**0.9114**
Image2	com	0.9732	0.7532	0.8250	*0.9891*	**0.9967**
	cor	0.5714	0.6014	**0.9762**	*0.9442*	0.9236
	q	0.5625	0.5024	0.8087	**0.9345**	*0.9208*
Image3	com	*0.9911*	0.9701	0.9250	0.9592	**0.9935**
	cor	0.7421	0.9151	**0.9534**	*0.9382*	0.9184
	q	0.7372	0.8900	0.8850	*0.9022*	**0.9129**
Avg(dataset)	com	*0.9353*	0.8578	0.8973	0.9228	**0.9427**
	cor	0.6827	0.8176	**0.9109**	*0.9078*	0.8946
	q	0.6505	0.7200	0.8249	*0.8437*	**0.8485**

TABLE II
TIME COMPARISONS OF DIFFERENT METHODS. HERE, THE TIME IS MEASURED IN SECONDS. Ct REFERS TO THE AVERAGE CLASSIFICATION TIME, AND Et REFERS TO THE AVERAGE CENTERLINE EXTRACTION TIME

	Image1		Image2		Image3	
size	1316*738		999*692		1232*735	
	Ct(s)	**Et**(s)	**Ct**(s)	**Et**(s)	**Ct**(s)	**Et**(s)
Huang	251.76	0.08	115.18	0.06	253.51	0.07
Miao	22.72	298.54	14.58	240.32	19.56	246.87
Shi	80.72	305.42	60.27	245.37	68.35	253.61
Cheng	249.70	247.51	197.35	190.35	235.73	195.73
Proposed	45.89	22.73	35.53	19.35	42.95	29.10

In the experiments, the number of labeled samples used in Huang's method and Cheng's method is 200 and 100, respectively, while the proposed method only need 60 labeled samples. Shi's method utilizes 5% of the number of all the pixels. It demonstrates that our semisupervised based method can achieve better performance with less labeled samples.

F. Time Comparison

The average running time among different methods in the classification stage and the centerline extraction stage is illustrated in Table II. All the experiments are conducted on a computer with Intel Core i5-3470 3.20-GHz CPU and 8-GB RAM using Matlab 2013. The result does not include the cross-validation time. As can be seen from the table, Miao's method and the proposed method take less time than the other three methods in the classification stage. Huang's method and Cheng's method take more time in this stage, and this is because they are multiscale-based methods. In the road centerline extraction stage, Huang's method takes the least time, but it produces short spurs around the centerline, thus reducing the smoothness and accuracy of the centerline. Miao's method, Shi's method, and Cheng's method cost more than ten times the running time of the proposed method. Thus, it demonstrates that the proposed method achieves relatively better performance with less running time than the other state-of-the-art methods.

IV. CONCLUSION

In this letter, a fast and easily implemented method has been proposed to extract road centerlines from remotely sensed imagery. In terms of both visual and quantitative performances, the proposed method achieves better results than all the other comparing methods. Moreover, the proposed road centerline extraction algorithm was ten times faster than those regression-based algorithms.

The proposed method can be also applied to other images, such as multispectral or hyperspectral images. However, there are some limits to the proposed method. First, the proposed method has good performance on rural roads and suburban roads, while for the other methods, the performance may decrease on the urban road images. Second, although the proposed method can connect the short discontinuity, it cannot effectively infer or connect the long discontinuity, which is an open question in the centerline extraction task.

REFERENCES

[1] M.-F. Auclair Fortier, D. Ziou, C. Armenakis, and S. Wang, "Survey of work on road extraction in aerial and satellite images," *Tech. Rep.*, vol. 24, no. 16, pp. 3037–3058, May 2003.
[2] J. B. Mena, "State of the art on automatic road extraction for GIS update: A novel classification," *Pattern Recognit. Lett.*, vol. 24, no. 16, pp. 3037–3058, Apr. 2003.
[3] A. Kaur and E. Ram Singh, "Various methods of road extraction from satellite images: A review," *Int. J. Res.*, vol. 2, no. 2, pp. 1025–1032, Nov. 2014.
[4] W. Shi, Z. Miao, and J. Debayle, "An integrated method for urban main-road centerline extraction from optical remotely sensed imagery," *IEEE Trans. Geosci. Remote Sens.*, vol. 52, no. 6, pp. 3359–3372, Jun. 2014.
[5] X. Huang and L. Zhang, "Road centreline extraction from high resolution imagery based on multiscale structural features and support vector machines," *Int. J. Remote Sens.*, vol. 30, no. 8, pp. 1977–1987, Apr. 2009.
[6] W. Shi, Z. Miao, Q. Wang, and H. Zhang, "Spectral-spatial classification and shape features for urban road centerline extraction," *IEEE Geosci. Remote Sens. Lett.*, vol. 11, no. 4, pp. 788–792, Apr. 2014.
[7] G. Cheng, Y. Wang, Y. Gong, F. Zhu, and C. Pan, "Urban road extraction via graph cuts based probability propagation," in *Proc. IEEE Int. Conf. Image Process.*, Oct. 2014, pp. 5072–5076.
[8] V. Mnih and G. E. Hinton, "Learning to detect roads in high-resolution aerial images," in *Proc. Eur. Conf. Comput. Vis.*, Sep. 2010, pp. 210–223.
[9] Z. Miao, W. Shi, H. Zhang, and X. Wang, "Road centerline extraction from high-resolution imagery based on shape features and multivariate adaptive regression splines," *IEEE Geosci. Remote Sens. Lett.*, vol. 10, no. 3, pp. 583–587, May 2013.
[10] F. Nie, H. Wang, H. Huang, and C. H. Q. Ding, "Adaptive loss minimization for semi-supervised elastic embedding," in *Proc. IJCAI*, Aug. 2013, pp. 1565–1571.
[11] D. Comaniciu and P. Meer, "Mean shift: A robust approach toward feature space analysis," *IEEE Trans. Pattern Anal. Mach. Intell.*, vol. 24, no. 5, pp. 603–619, May 2002.
[12] G. Cheng, F. Zhu, S. Xiang, and C. Pan, "Accurate urban road centerline extraction from VHR imagery via multiscale segmentation and tensor voting," submitted for publication. [Online]. Available: http://arxiv.org/abs/1508.06163.
[13] M. Dalla Mura, J. Benediktsson, B. Waske, and L. Bruzzone, "Extended profiles with morphological attribute filters for the analysis of hyperspectral data," *Int. J. Remote Sens.*, vol. 31, no. 22, pp. 5975–5991, Dec. 2010.
[14] W. Dong, M. Charikar, and K. Li, "Efficient k-nearest neighbor graph construction for generic similarity measures," in *Proc. WWW*, Apr. 2011, pp. 577–586.
[15] C. Heipke, H. Mayer, C. Wiedemann, and O. Jamet, "Evaluation of automatic road extraction," in *Proc. Int. Arch. Photogramm. Remote Sens.*, Feb. 1997, pp. 47–56.
[16] B. Wessel and C. Wiedemann, "Analysis of automatic road extraction results from airborne SAR imagery," in *Proc. ISPRS Arch.*, Sep. 2003, pp. 105–110.